

---

# Loss Landscape Geometry and the Learning of Symmetries: Or, What Influence Functions Reveal About Robust Generalization

---

James Amarel<sup>1</sup> Robyn Miller<sup>1</sup> Nicolas Hengartner<sup>1</sup> Benjamin Migliori<sup>1</sup> Emily Casleton<sup>1</sup> Alexei Skurikhin<sup>1</sup>  
Earl Lawrence<sup>1</sup> Gerd J. Kunde<sup>1</sup>

## Abstract

We study how neural emulators of partial differential equation solution operators internalize physical symmetries by introducing an influence-based diagnostic that measures the propagation of parameter updates between symmetry-related states, defined as the metric-weighted overlap of loss gradients evaluated along group orbits. This quantity probes the local geometry of the learned loss landscape and goes beyond forward-pass equivariance tests by directly assessing whether learning dynamics couple physically equivalent configurations. Applying our diagnostic to autoregressive fluid-flow emulators, we show that orbit-wise gradient coherence provides the mechanism for learning to generalize over symmetry transformations and indicates when training selects a symmetry compatible basin. The result is a novel technique for evaluating if surrogate models have learned symmetry properties of the known solution operator.

## 1. Introduction

Deep learning emulators for partial differential equation (PDE) solvers routinely achieve impressive in-distribution accuracy (Brandstetter et al., 2023; Herde et al., 2024; Takamoto et al., 2024; Lippe et al., 2023; Gupta & Brandstetter, 2022; Ohana et al., 2025), yet they often fail to respect the fundamental symmetries of the governing equations (Akhound-Sadegh et al., 2023; Gregory et al., 2024; Gruver et al., 2022). This limitation undermines their ability to extrapolate and generalize, raising the question: are such models truly learning physics, or merely fitting correlations present in the training data? Explaining this gap requires probing not just the outputs, but also the learning dynamics (Fort et al., 2020; Zhao et al., 2024).

<sup>1</sup>Los Alamos National Laboratory, Los Alamos, NM 87545. Correspondence to: James Amarel <jlamarel@lanl.gov>.

Preprint. January 29, 2026.

Symmetries of the Navier-Stokes equations, namely translations, rotations, reflections, scalings, and Galilean boosts, organize the solution space into orbits whose members are physically equivalent (Brandstetter et al., 2022). A model that has internalized the solution operator will propagate information seamlessly across these orbits: gradients of the loss with respect to parameters, evaluated on symmetry-related inputs, should align, on account of equivariance; without such coherence, the resulting loss differentials do not constructively influence one another, rendering the orbit decoupled. Measuring cross-influence offers a diagnostic beyond standard forward-pass equivariance checks, exposing the degree to which training updates are physically consistent.

If influence across group actions presents only weakly, the model is memorizing localized patterns rather than learning physical processes (Arpit et al., 2017; He & Su, 2020; Chatterjee, 2020). Conversely, persistent gradient coherence signals that the network has learned to couple symmetry-related states, consistent with the behavior of a true solution operator. Our symmetry-aware gradient diagnostic therefore quantifies a model’s ability to generalize across orbits, providing a principled tool to assess how architectural choices, loss design, and inductive biases promote, or hinder, robust generalization.

## 2. Contributions

Our work contributes to three core themes of contemporary machine learning research. First, it advances interpretability methods by using influence functions to directly probe training dynamics, going beyond an analysis of forward-pass behavior alone. Second, it informs generalization theory by framing symmetry learning as a problem of basin selection in the loss landscape, governed by orbit-wise gradient coherence. Third, within scientific machine learning, it provides a principled diagnostic for assessing if neural emulators have genuinely learned symmetries of the underlying solution operator.

We extend a previously developed gradient-based explainability framework (Anonymous, 2026) to determine why data-driven PDE emulators often fail to learn and exploit

physical symmetries. We introduce a geometry-aware, symmetry-conditioned gradient-influence diagnostic that probes how training updates propagate across symmetry group orbits, specifically the dihedral group of rotations and reflections, in addition to specific discrete translations. Our diagnostic is architecture- and domain-agnostic, provided gradients and group actions are defined. We pair this gradient alignment analysis with forward pass equivariance error tests to produce a coherent audit of symmetry learning. This study of how gradient coherence facilitates the flow of information through a group orbit supplements prediction-based evaluation metrics by determining if the underlying learning dynamics that govern generalization are symmetry-compatible. This analysis reveals that disrespect of symmetry may present not only in representation space but also in the local geometry, which need not support a coherent update structure across symmetry-related inputs. Furthermore, our results shed light on the trade-off between using bespoke architectures to enforce symmetry and the ease of training a flexible model.

In this work, generalization refers to the standard notion of test-risk on unseen data; our focus is on equivariance consistency and its mechanistic underpinnings. The proposed orbit-wise gradient coherence is a local property of the trained model’s loss landscape. Exact equivariance implies uniform coherence, but the converse need not hold, making coherence a necessary but not sufficient indicator of symmetry learning. We therefore use coherence as a diagnostic that training updates couple symmetry-related states, and we relate it empirically to forward equivariance error across dihedral and translational transformations. Together, these components provide a concise framework for evaluating symmetry-consistent behavior via both forward-pass consistency and probes of the learning dynamics, including settings where equivariance is only approximate or is learned implicitly by flexible backbones.

### 3. Method

We compare a UNet (13M parameters, 4 down-sampling blocks, 24 embedding channels) and a Vision Transformer (ViT; 5M parameters, 6 layers, 256 channels) trained as emulators for two-dimensional compressible Euler flows from PDEGym (Herde et al., 2024). For data, we selected three classes of Riemann-type initial conditions (CE-RP, CE-RPUI, CE-CRP), each with 5,000 trajectories of 16 time steps. Each state snapshot is a  $128 \times 128$  grid of mass density, Cartesian momentum density, and energy density. Models were trained autoregressively to emulate the Euler evolution operator. To complement the compressible Euler results, we also apply our analysis to models trained on velocity fields generated by the Navier-Stokes (NS) equations using, NS-BB, NS-Gauss, and NS-Sines initial conditions.

These flows occupy a qualitatively different feature space, characterized by smoother, viscosity-regularized dynamics and vorticity-dominated structure.

Optimization used Adam with learning rate  $5 \times 10^{-4}$  and weight decay  $\lambda = 10^{-6}$  on mini-batches of  $N = 48$  transitions. The cost function was a scaled mean-squared error (SMSE), that normalizes errors by channel RMS to balance large and small-amplitude features, ensuring shocks and wavefronts are captured while retaining sensitivity to quiescent flows, in addition to rendering dimensionless the influence matrix of interest. Both models were trained in distributed mode on two 40GB A100 GPUs using Lux.jl (Pal, 2023b;a) and Zygote.jl (Innes, 2018), with three seeds controlling initialization and dataset splits. Results are reported with quantile range bars to capture variability across seeds and mini-batches. Despite having fewer parameters, our ViTs consistently outperforms our UNets on test metrics. Technical details regarding both model training and the forthcoming mathematical analysis can be found in our companion paper (Anonymous, 2026).

To evaluate our models, we compute the influence function, which can be expressed as the Lie derivative of the cost along gradient directions induced by individual test examples. Let  $V^\mu = -\chi^{\mu\nu} \partial_\nu C_x$  denote the vector field generated by the loss evaluated on an example  $x$ . The influence of this update on the loss evaluated at the transformed input  $gx$  is given by

$$\mathcal{L}_V C_{gx} = (\partial_\mu C_{gx}) \chi^{\mu\nu} (-\partial_\nu C_x), \quad (1)$$

where  $\chi_{\mu\nu} = \eta_{\mu\nu} + \lambda \delta_{\mu\nu}$  is the regularized neural tangent kernel metric (Jacot et al., 2020), and  $\chi^{\mu\nu}$  denote the elements of  $\chi^{-1}$  (Absil et al., 2008). Einstein summation convention is implicit and we use standard index raising notation from differential geometry. Equation 1 recovers the familiar influence function definition as a metric-weighted overlap between gradients derived from the cost evaluated on an example  $x$  and the transformed counterpart  $gx$  (Fort & Ganguli, 2019). Intuitively, the influence function measures whether a gradient update induced by one example decreases (or increases) the loss of another. When applied to symmetry-related inputs, it quantifies whether learning signals propagate coherently along symmetry orbits.

In regression, the neural tangent kernel plays the role of a Fisher-information analog by supplying the Jacobian-induced metric on parameter space (Martens, 2020). For each model seed, the influence function is evaluated across six test mini-batches comprising full trajectories for each of the three training-time classes of initial conditions. The resulting influence matrices are standardized (Lu et al., 1997; Héritier & Ronchetti, 1994) by normalizing with respect to the empirical variance of perturbations in each mini-batch, so that unity defines the natural baseline associated with unstructured stochastic variability. Deviations from this scale

therefore quantify influence beyond random training noise, enabling principled interpretation of both self- and cross-response structure. In practice,  $\chi$  is applied via a Krylov.jl (Montoisson & Orban, 2023) matrix-free solver, yielding a measure of gradient alignment sensitive to the local geometry of the loss surface (Fort & Ganguli, 2019; Zielinski et al., 2020)

Note that accurate evaluation of influence matrices in the  $\chi$ -metric for an entire mini-batch requires solving large linear systems to low residual tolerance, which incurs substantial computational cost. As a result, our measurements are restricted to local probes of the loss landscape in the late-stage training basin, rather than being tracked throughout optimization. In particular, we do not compute the full normalization required to form cosine angles between gradients, as this would necessitate repeated high-accuracy inversions of  $\chi$ . Furthermore, metric-weighted inner products better capture the local loss geometry than, e.g., cosine-stiffness. Because of this constraint, prior work has typically relied on uncontrolled approximations to the curvature or influence geometry (TransferLab, 2024; George, 2021; Martens & Grosse, 2020). On the contrary, we have full control over the relative tolerance parameter in our linear solves (Anonymous, 2026).

## 4. Results

Our evaluation jointly considers equivariance error, which probes forward-pass consistency under symmetry transformations, and influence function matrix elements, which quantify the alignment of parameter updates induced by symmetry-related inputs. The influence function reveals whether learning dynamics propagate information coherently across symmetry-related states, exposing whether a model is genuinely learning physics or merely fitting data. Convergence to basins that respect the symmetries of the underlying problem is both essential for generalization and a persistent challenge for current architectures. Throughout this section, we test the central hypothesis that forward-pass equivariance emerges precisely when training dynamics propagate gradient information coherently along symmetry orbits. We find that forward-pass equivariance error is characterized by the extent to which our models internalize symmetry-coherent gradients.

We begin by analyzing symmetry learning with respect to the dihedral group  $D_4$ , the set of discrete rotations and reflections admissible under the Navier–Stokes dataset used for training. Our models successfully generalize on those group transformations for which gradients are propagated coherently through the loss landscape. Where generalization fails, we show that training dynamics do not support full orbit-wise coupling and visualize how data-induced anisotropies are absorbed into the learned loss landscape

geometry.

Next, we consider the translation group. In this case, our UNets exhibit constructive gradient coherence that is nearly uniform. On the other hand, our ViTs distribute influence non-uniformly but support larger influence on privileged group elements. These observations highlight a trade-off between inductive bias and optimization flexibility. Enforcing uniform coupling across all group elements can constrain the space of admissible update directions and, in some settings, impede optimization (Zhang, 2019; Azulay & Weiss, 2019; Kayhan & van Gemert, 2020) by inducing a mean gradient direction that is inconsistent with individual update directions, otherwise known as type-II gradient misalignment (Wang et al., 2025). In our translation group related experiments, we observe exclusively positive influence values, indicating that updates are not antagonistic across group elements. The absence of negative influence indicates that optimization does not suffer from conflicting updates across group elements; instead, the distinction lies in how learning signal is distributed: architectures with weaker inductive bias are free to concentrate influence on a subset of symmetry transformations, enabling rapid convergence via a strong gradient response, but limiting generalization capabilities across the group. This contrast illustrates how architectural constraints can promote principled symmetry learning at the cost of optimization flexibility, while unconstrained models optimize efficiently yet may only partially internalize the symmetry structure, motivating approximately constrained approaches that balance these effects (Wang et al., 2022).

Convergence to loss basins that respect the symmetries of the underlying PDE is essential for robust generalization, yet remains a persistent challenge for current architectures. The following results demonstrate that influence functions provide a direct probe of this phenomenon by revealing whether learning dynamics couple physically equivalent states.

### 4.1. Dihedral Group

We first analyze the failure of our Navier-Stokes trained models to internalize the action of the dihedral group  $D_4$ , a breakdown that presents across random seeds and mini-batches despite otherwise excellent pointwise accuracy and low untransformed test loss [see Figure 1]. Both architectures achieve competitive performance on the identity element  $e$ , 180 degree rotations  $r^2$ , 90 degree rotations followed by a flip about the vertical axis  $sr$ , and 270 degree rotations followed by such a flip  $sr^3$ , yet their response under the remaining group actions reveals a sharp and systematic lack of symmetry adherence. In this case, the relative SMSE increases catastrophically, by nearly  $10^4$ , indicating that the learned predictors are not even approximately equivariant when all group actions are considered. Such behavior is not

entirely unexpected. The Navier-Stokes dataset carries a pronounced directional bias in feature space, inherited from the choice of initial conditions and the anisotropic, vorticity-dominated structure of the flows that is not invariant under reflections or 90 degree rotations. What is striking, however, is that the symmetry breaking is not merely a property of the forward map. The influence structure associated with these unlearned group actions is distinguished [see Figure 2]. Crucially, the group elements with catastrophic equivariance error are precisely those with suppressed cross-influence.

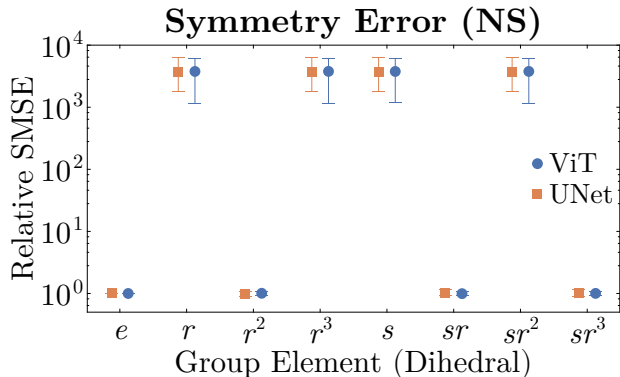


Figure 1. Dihedral group equivariance error on Navier-Stokes (NS) data. Relative SMSE evaluated on NS trajectories. Points denote medians over seeds and test examples; ranges indicate variability. Deviations from unity quantify dihedral symmetry breaking. For the analogous result involving CE data, see Figure 9.

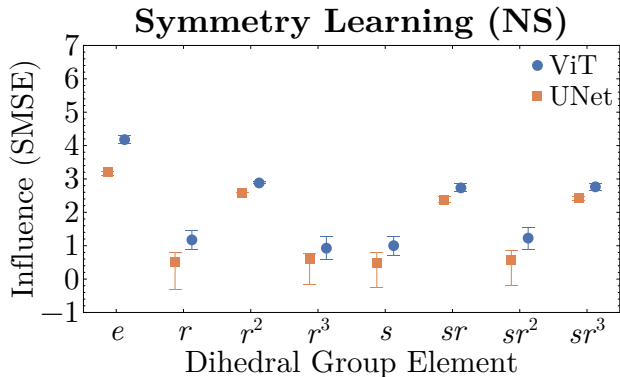


Figure 2. Dihedral group influence on NS data. Influence between an input and its square group rotated state on NS data. Points denote medians; ranges summarize inter-seed and inter-example variability, measuring coupling of learning dynamics along dihedral orbits. For the analogous result involving CE data, see Figure 10.

Rather than providing a democratic sharing of coupling across the dihedral orbit, optimization drove our models into a region of the loss landscape that displays a clear demarcation between well-learned and challenging group elements, with the latter receiving subdominant influence.

Notably, our UNets assign such challenging rotations near-zero cross-influence, even though these out-of-distribution (but physically permissible) transformations induce large gradients, indicating that training has converged to a basin with symmetry-incompatible geometry. We emphasize that although the dihedral symmetry is physically valid and symmetry-transformed inputs generate large gradients, gradient signals do not accumulate coherently over symmetry operations. Instead, data-induced anisotropies are absorbed into the local loss geometry, inducing training dynamics that reinforce symmetry-breaking. Such rotations are in-distribution under reasonable deployment assumptions, meaning that the observed decoupling reflects a zero-shot generalization gap between model performance on the training distribution and the operational distribution, indicating limited ability to generalize over the full data manifold.

In an equivariant learning regime, influence is allocated comparably across all group actions, reflecting a training flow that symmetrically propagates learning signals over the orbit. That our UNets exhibit an incoherent response to certain symmetry operations, whereas our ViTs accommodate a consistent but weak response in these directions, highlights a difference in how the two architectures accommodate dihedral symmetry within their respective loss basins. Although, in both cases, the observed influence hierarchy reflects optimization dynamics that internalize a preferred orientation inherited from the data. Our test-time probes interrogate directions that are poorly aligned with the primary drift direction traced by the training flow. Hence, symmetry-related gradient signals enter only as subleading perturbations and fail to accumulate coherently, explaining how models achieve excellent pointwise accuracy on in-training-distribution data while converging to basins whose local geometry explicitly breaks dihedral symmetry.

Together, Figure 1 and Figure 2 resolve the apparent tension between low in-training-distribution test error and severe dihedral failure: under symmetry-agnostic training, the induced training dynamics do not propagate information across the entire  $D_4$  orbit; consequently, neither model class achieves generalization over symmetry transformations, a necessary property for learning the underlying solution operator.

Our CE-trained models exhibit low square-group equivariance error [see Figure 9], accompanied by an influence profile that is distributed approximately uniformly across the  $D_4$  orbit [see Figure 10]. This behavior is consistent with the symmetry operations being adequately represented within the training distribution, such that symmetry-agnostic optimization nevertheless induces orbit-wise coupling in the learned response geometry. This observation suggests that influence-based diagnostics can be used to reason about minimal data augmentation strategies.

## 4.2. Translation Group

For the translation group, we first evaluate purely horizontal and vertical translations across the full periodic spatial domain. Because the governing PDE applies uniformly in space, the learned dynamics should be equivariant under translations. In any given flow snapshot, nonlinear interactions occupy only a small number of localized regions, yet these structures may arise at arbitrary spatial locations. A model that learns translational equivariance will therefore treat such interactions consistently wherever they occur, a prerequisite for both capturing rare but dynamically significant events and enabling accurate long-time extrapolation.

Both architectures exhibit median relative equivariance error on the order of one percent or less, indicating that training largely confers translational symmetry generalizing capabilities. Notably, the relative equivariance error attained by our models [see Figure 3 and Figure 4] reflects genuine generalization over the translation group: we did not explicitly augment the training data with translated states, nor was either architecture designed to enforce exact equivariance over the entire translation group under consideration. In particular, translation invariance is violated by the distribution from which four quadrant initial conditions for both CE-RP and CE-RPUI flows were drawn. Nevertheless, we observe nontrivial cross-influence across translated states, indicating that training updates partially couple translation-related inputs, even without hard symmetry constraints. For this reason, we focus on the third quantile (Q3) when reporting translation equivariance error, which isolates cases with pronounced symmetry violation and exhibits a striking correspondence with the measured influence across translations. Focusing on the upper tail isolates examples for which translational symmetry is most weakly supported, making clear the relation between forward-pass failures and heterogeneity in the underlying gradient coupling. Indeed, the Q3 error profiles present differences across architectures and anisotropic peculiarities that can be better understood when forward pass error is supplemented with influence function analysis [see Figure 5 and Figure 6].

For our ViTs, the translation response exhibits a pronounced axis-dependent resonance structure. Under horizontal (vertical) translations, the a periodicity of wavelength 16 (32) pixels indicates that the measured influence/equivariance observables couple anisotropically to the phase of the translation relative to the patch lattice, with different group elements emphasized in different directions. This axis-dependent anisotropy is consistent with a representational bias introduced by flattening the two-dimensional patch grid into a one-dimensional token sequence. While the patch embedding itself is convolutional of stride four, the subsequent permutation into tokens and channel mixing allows for a preferred ordering on spatial degrees of freedom, thereby

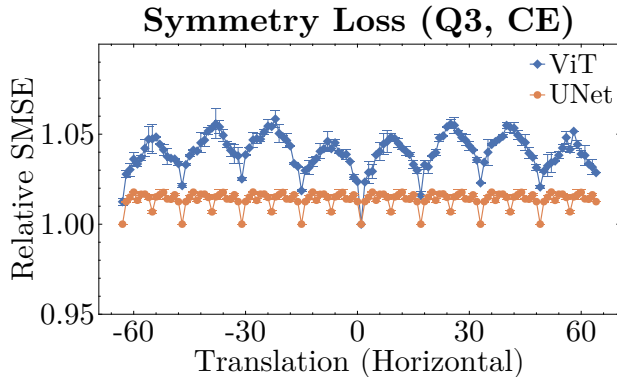


Figure 3. Horizontal-translation equivariance error on CE data. Third-quantile (Q3) relative SMSE as a function of horizontal translation. Markers denote medians across seeds; ranges summarize variability over seeds and test examples, emphasizing upper-tail symmetry breaking. For analogous results with NS data, see Figure 13.

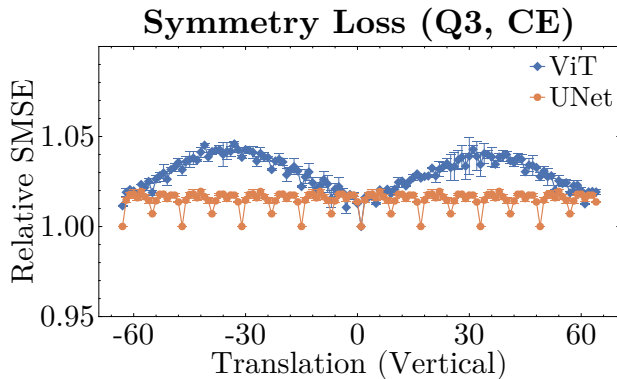


Figure 4. Vertical-translation equivariance error on CE data. Third-quantile relative SMSE under vertical translations. Markers denote medians across seeds; ranges summarize inter-seed and inter-example variability, isolating upper-tail error under symmetry perturbations. For analogous results with NS data, see Figure 12.

breaking the manifest equivalence between horizontal and vertical directions, which impacts the learned response geometry.

In contrast, our UNets employ convolutional operators across contracting and expanding resolutions, with four down-sampling stages. The coarsest representation has spatial extent  $8 \times 8$ , which promotes a comparatively smooth dependence of influence on translation, with only low-amplitude variation at shorter 8 pixel wavelengths and their subharmonics. Consistent with this architecture-level partial symmetry adherence, UNets exhibit similar influence profiles across horizontal and vertical translations.

In both cases, inspection of both forward-pass equivariance error and influence profile provides an explanatory mechanism for symmetry learning: resonant minima in the error profile coincide with structured extrema in the response,

and vice-versa. Nevertheless, both models support cross-influence above the unit baseline, indicating that the learned response geometry supports nontrivial propagation across the translation orbit and thus generalization over translations, even in the absence of explicit translation augmentation or exact equivariance constraints.

Sporadic coupling over the group allows our ViTs to concentrate each learning signal on a subset of translation phases, producing stronger local responses at the cost of more heterogeneous orbit-wise coupling. Less rigid coupling between translation elements for the ViT may be advantageous when paired with an overall larger peak response, as its updates are flexibly dispersed throughout the group.

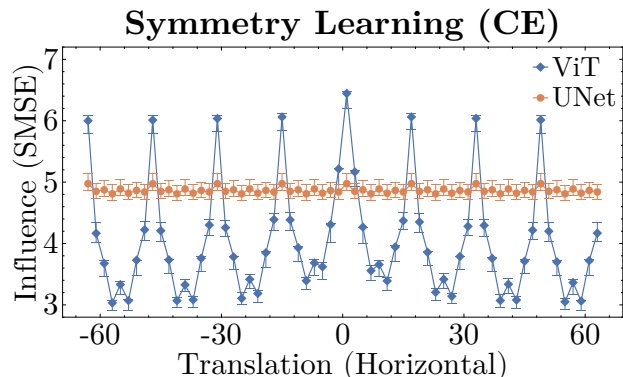


Figure 5. Horizontal-translation influence on CE data. Influence between an input and its horizontally translated state; structured dependence on translation distance reveals spatial coupling of learning dynamics. Markers denote medians; ranges indicate variability over seeds and test examples. For analogous results with NS data, see Figure 11.

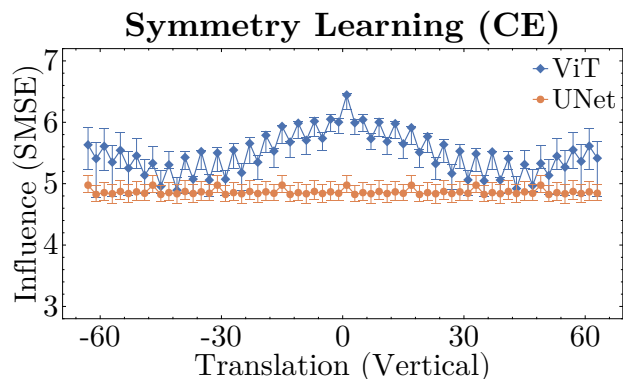


Figure 6. Vertical-translation influence on CE data. Same as the horizontal case, but for vertical shifts. Comparison with horizontal translations of Figure 5 reveals anisotropy in symmetry-coupled learning. Markers denote medians; ranges indicate variability over seeds and test examples. For analogous results with NS data, see Figure 14.

Beyond purely horizontal and vertical shifts, we also evalu-

ate joint translations over a subset of the two-dimensional translation group. Figure 7 shows the resulting translation-equivariance error landscape for the ViT on CE data, while Figure 8 reports the corresponding influence landscape over the same grid. Together, these plots reveal that translation-induced symmetry breaking is organized into smooth, structured regions on the translation torus. Patterns in the forward-pass error align closely with features in the influence landscape: regions exhibiting elevated Q3 equivariance error coincide with translations for which parameter-update coupling is weak. This correspondence reinforces the interpretation that influence captures the effective resolution at which the model distinguishes translations. Given the periodic response exhibited by our models, we expect that this sub-sampling suffices to expose the geometry of translation generalization, without requiring exhaustive evaluation over the full  $\mathbb{Z}_{128} \times \mathbb{Z}_{128}$  orbit. Indeed, the translation action is

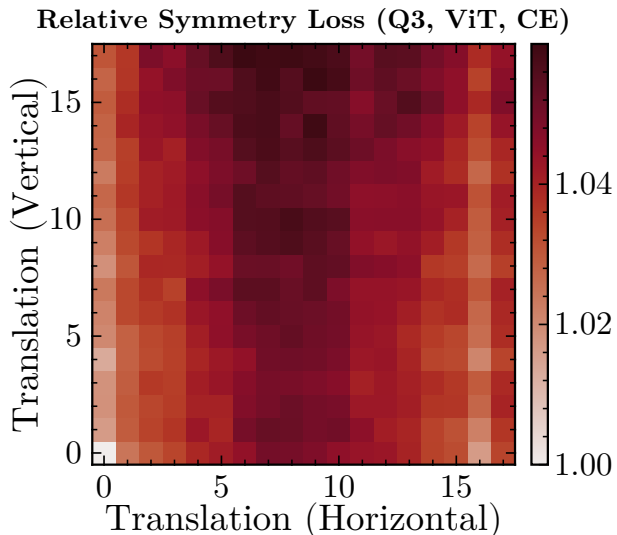


Figure 7. Translation-equivariance error landscape for ViT on CE data. Heatmap of third-quantile relative SMSE as a function of joint horizontal and vertical translations. Color encodes the magnitude of translation-induced symmetry breaking in the forward error. For analogous results with NS data, see Figure 20.

discrete and the influence curves are periodic, hence the full augmentation orbit  $\mathbb{Z}_{128} \times \mathbb{Z}_{128}$  is massively redundant from the perspective of the learned response geometry. For data augmentation derived symmetry learning, our diagnostics suggest that exhaustive enumeration of over the full translation group may be unnecessary, one need only verify that unsampled translations lie in the same response-equivalence classes.

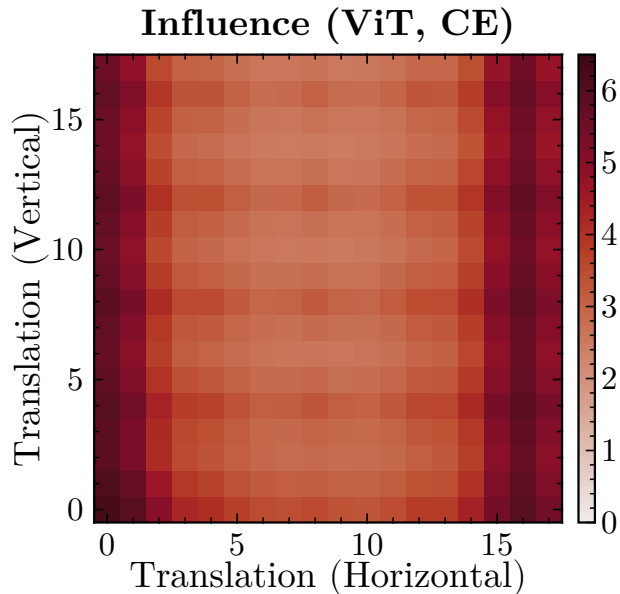


Figure 8. Translation-group influence landscape for ViT on CE data. Heatmap of influence between an input and its translated state over the translation grid. Color encodes the strength of parameter-update coupling across translated states. For analogous results with NS data, see Figure 19.

## 5. Related Work

Encoding symmetries as inductive biases has a long tradition in geometric deep learning. Group-equivariant CNNs generalize convolution to arbitrary groups with weight sharing across orbits (Cohen & Welling, 2016). Steerable CNNs make these ideas explicit by parameterizing kernels in group-steerable bases, including variants for volumetric data (Cohen & Welling, 2017; Weiler et al., 2018). For non-grid domains, tensor field networks (Thomas et al., 2018) and E(n)-equivariant graph neural networks (Garcia Satorras et al., 2021) extend manifest symmetry compliance to point clouds and molecules. In practice, scientific data rarely obey exact symmetries; boundary conditions, material inhomogeneities, grid discretization, and measurement noise introduce systematic symmetry breaking. This motivates research into approximate (Wang et al., 2022) and relaxed (Finzi et al., 2021) attainment of equivariance. Furthermore, contemporary large-scale weather and climate models such as Aurora (Bodnar et al., 2024) and ClimaX (Nguyen et al., 2023) rely on data-driven learning of symmetry. Empirical and theoretical results substantiate this strategy: softening hard constraints can improve optimization and accuracy (Wang et al., 2022). Relatedly, classic studies show that modern CNNs can be brittle to small shifts and rotations (Azulay & Weiss, 2019; Zhang, 2019; Kayhan & van Gemert, 2020).

In cases where a model lacking manifest symmetry is selected, probes are needed to both quantify and explain

the degree of equivariance achieved after training. Several diagnostics test whether models learn symmetry, e.g., forward-pass checks to evaluate equivariance error under group actions (Canez et al., 2024; Xie & Smidt, 2025) and the Lie derivative metric, which quantifies infinitesimal equivariance with layerwise decomposition (Gruver et al., 2022). Yet, spot tests with these metrics are insufficient to explain the mechanism underlying symmetry learning. Such diagnostics characterize equivariance of the learned map, but do not reveal whether training dynamics actually propagate information across symmetry-related states. To better understand the degree to which a given model exhibits equivariance, one can relate observed behavior to architectural choices and training dynamics.

A central approach in explainable AI is to interrogate the loss and its derivatives to connect predictive behavior with training signals. Related work on gradient geometry links cross-example parameter update structure to out-of-sample performance: stiffness and coherent gradients capture alignment, and local elasticity studies stability under SGD updates on distant samples (Fort et al., 2020; Chatterjee, 2020; He & Su, 2020). Euclidean influence functions trace predictions to training data but are delicate in deep, non-convex regimes, motivating curvature-aware variants (Koh & Liang, 2020; Basu et al., 2020; Jacot et al., 2020; Fort & Ganguli, 2019).

To our knowledge, this work is the first to analyze symmetry learning through the lens of influence functions, measuring how parameter updates induced by an input propagate to its symmetry-transformed counterparts. Unlike prior diagnostics that evaluate equivariance at the level of the learned map, our approach probes whether training dynamics themselves propagate information across symmetry orbits.

## 6. Limitations

Certain physically relevant symmetries remain outside the scope of the present study. Galilean boosts, in particular, impose a highly restrictive constraint: exact equivariance can be achieved only by affine transformations, while generic nonlinear architectures can at best satisfy this symmetry approximately (Wang et al., 2022). It would be interesting to extend our influence-based analysis to probe the response under small Galilean boosts. We did not examine the scaling symmetry of the continuum Navier-Stokes equations. In practical settings this symmetry is generically broken by spatial discretization, numerical regularization, and coarse graining of the data, rendering its faithful assessment ambiguous within the present framework. Finally, our empirical analysis is limited to UNet and ViT architectures, chosen as representative backbones of foundation models widely used in scientific machine learning. For architectures that enforce exact equivariance by construction, influence across

symmetry orbits would be uniform by design. While such architectures guarantee symmetry by construction, they do not address whether symmetry can be learned implicitly under realistic data and optimization constraints, which is the regime targeted by modern large-scale scientific models. Our focus is therefore on settings in which symmetry learning is implicit and contingent on training dynamics rather than guaranteed a priori. Furthermore, our diagnostics characterize symmetry learning relative to the training distribution; when symmetry transformations are poorly represented in data, influence-based measures reflect this bias rather than an intrinsic architectural limitation.

## 7. Conclusion

Our analysis sharpens recent insights on the interplay between inductive bias, optimization, and symmetry learning (Canez et al., 2024). We show that test time equivariance error is determined by how training dynamics distribute influence across group orbits. While symmetry-agnostic architectures can attain low test error, such models allow for disparate allocation of influence across orbits, producing solutions that interpolate accurately yet fail to internalize the structure of the underlying solution operator.

On two PDE emulation tasks, our ViTs converged rapidly, but did so with freely specialized gradients, leading to strong on-diagonal responses that sacrifice faithful symmetry representation. In this regime, low test error coexists with idiosyncratic orbit-wise coupling, signaling convergence to symmetry-incompatible basins: the result is high predictive accuracy but limited physical consistency, characteristic of powerful interpolators rather than genuine physics emulators; apparent accuracy in the absence of gradient coherence is an indicator of reduced robustness under symmetry transformations. By contrast, manifestly equivariant group convolution layers, such as those in UNets, promote data efficiency and principled generalization through uniform gradient coupling across symmetry orbits, but this rigidity can slow convergence and hinder optimization. Even when typical equivariance errors are relatively low, we find that model failure to respect symmetry on select challenging examples is explainable by a lack of coherent orbit-wise gradient sharing, indicating a failure of the symmetry learning mechanism to apply wholly across the dataset.

By explicitly measuring cross-influence between symmetry-related states, our framework reveals whether learning dynamics propagate information coherently along an orbit or instead distribute influence in a way that precludes convergence to generalizing solutions. This provides a novel diagnostic for distinguishing models that learn to exploit shared structure from those that effectively assemble collections of local estimators. Tying symmetry generalization directly to the geometry of the learned loss landscape com-

plements standard equivariance accuracy metrics and provides a clearer criterion for when apparent performance reflects genuine physics learning. Such diagnostics are essential for building trust in scientific machine learning systems, particularly in applications requiring robustness under symmetry transformations. Looking forward, this perspective motivates the development of approximate or relaxed symmetry mechanisms that retain sufficient structure to guide generalization while preserving the flexibility needed for efficient optimization, potentially reconciling the scalability of transformers with the principled foundations of equivariant modeling.



## 8. Electronic Submission

### Software and Data

We trained our models on the openly available dataset PDE-Gym (Herde et al., 2024) using Lux.jl (Pal, 2023b;a), with Zygote.jl as our auto-differentiation backend (Innes, 2018). Plots in this manuscript were generated using Makie.jl (Danisch & Krumbiegel, 2021).

The code used in this work is publicly available at <https://anonymous.4open.science/r/PDEHats-B7BF/>. Additionally, trained models and gradient data are available from the authors upon reasonable request.

### Acknowledgements

Research presented in this report was supported by the Laboratory Directed Research and Development program of Los Alamos National Laboratory under project number(s) 20250637DI, 20250638DI, and 20250639DI. This research used resources provided by the Los Alamos National Laboratory Institutional Computing Program, which is supported by the U.S. Department of Energy National Nuclear Security Administration under Contract No. 89233218CNA000001. It is published under LA-UR-25-29466.

### Impact

This work aims to strengthen trust in scientific machine learning by clarifying when models truly learn physics, while also underscoring the risks of misuse if surrogate predictions are deployed without such diagnostic safeguards. Our diagnostics provide a practical tool for interpreting and validating scientific machine learning models, advancing the explainable artificial intelligence agenda of probing and re-engineering model behavior to foster knowledge-driven development.

### References

- Absil, P.-A., Mahony, R., and Sepulchre, R. *Optimization Algorithms on Matrix Manifolds*. Princeton University Press, Princeton, NJ, 2008. ISBN 978-0-691-13298-3.
- Akhound-Sadegh, T., Perreault-Levasseur, L., Brandstetter, J., Welling, M., and Ravanbakhsh, S. Lie point symmetry and physics informed networks, 2023. URL <https://arxiv.org/abs/2311.04293>.
- Anonymous. Generalization vs. memorization in autoregressive deep learning: Or, examining temporal decay of gradient coherence, 2026. URL <https://anonymous.4open.science/r/PDEHats-B7BF/>.
- Arpit, D., Jastrzebski, S., Ballas, N., Krueger, D., Bengio, E., Kanwal, M. S., Maharaj, T., Fischer, A., Courville, A., Bengio, Y., and Lacoste-Julien, S. A closer look at memorization in deep networks, 2017. URL <https://arxiv.org/abs/1706.05394>.
- Azulay, A. and Weiss, Y. Why do deep convolutional networks generalize so poorly to small image transformations? *Journal of Machine Learning Research*, 20(184):1–25, 2019. URL <http://jmlr.org/papers/v20/19-519.html>.
- Basu, S., You, X., and Feizi, S. On second-order group influence functions for black-box predictions. In *Proceedings of the 37th International Conference on Machine Learning*, volume 119 of *PMLR*, pp. 715–724, 2020. URL <https://proceedings.mlr.press/v119/basu20b.html>.
- Bodnar, C., Bruinsma, W. P., Lucic, A., Stanley, M., Vaughan, A., Brandstetter, J., Garvan, P., Riechert, M., Weyn, J. A., Dong, H., Gupta, J. K., Thambiratnam, K., Archibald, A. T., Wu, C.-C., Heider, E., Welling, M., Turner, R. E., and Perdikaris, P. A foundation model for the earth system, 2024. URL <https://arxiv.org/abs/2405.13063>.
- Brandstetter, J., Welling, M., and Worrall, D. E. Lie point symmetry data augmentation for neural PDE solvers. In Chaudhuri, K., Jegelka, S., Song, L., Szepesvari, C., Niu, G., and Sabato, S. (eds.), *Proceedings of the 39th International Conference on Machine Learning*, volume 162 of *Proceedings of Machine Learning Research*, pp. 2241–2256. PMLR, 17–23 Jul 2022. URL <https://proceedings.mlr.press/v162/brandstetter22a.html>.
- Brandstetter, J., Worrall, D., and Welling, M. Message passing neural pde solvers, 2023. URL <https://arxiv.org/abs/2202.03376>.
- Canez, D., Midavaine, N., Stessen, T., Fan, J., Arias, S., and Garcia, A. Effect of equivariance on training dynamics, 2024. URL <https://gram-blogposts.github.io/blog/2024/relaxed-equivariance/>.
- Chatterjee, S. Coherent gradients: An approach to understanding generalization in gradient descent-based optimization, 2020. URL <https://arxiv.org/abs/2002.10657>.
- Cohen, T. S. and Welling, M. Group equivariant convolutional networks. In *Proceedings of the 33rd International Conference on Machine Learning*, volume 48 of *PMLR*, pp. 2990–2999, 2016. URL <https://proceedings.mlr.press/v48/cohen16.pdf>.
- Cohen, T. S. and Welling, M. Steerable CNNs. In *ICLR*, 2017. URL <https://arxiv.org/abs/1612.08498>.

- Danisch, S. and Krumbiegel, J. Makie.jl: Flexible high-performance data visualization for Julia. *Journal of Open Source Software*, 6(65):3349, 2021. doi: 10.21105/joss.03349. URL <https://doi.org/10.21105/joss.03349>.
- Finzi, M., Benton, G., and Wilson, A. G. Residual pathway priors for soft equivariance constraints, 2021. URL <https://arxiv.org/abs/2112.01388>.
- Fort, S. and Ganguli, S. Emergent properties of the local geometry of neural loss landscapes, 2019. URL <https://arxiv.org/abs/1910.05929>.
- Fort, S., Nowak, P. K., Jastrzebski, S., and Narayanan, S. Stiffness: A new perspective on generalization in neural networks, 2020. URL <https://arxiv.org/abs/1901.09491>.
- Garcia Satorras, V., Hoogeboom, E., and Welling, M. E(n) equivariant graph neural networks. In *Proceedings of the 38th International Conference on Machine Learning*, volume 139 of *PMLR*, pp. 9323–9332, 2021. URL <https://proceedings.mlr.press/v139/satorras21a.html>.
- George, T. NNGeometry: Easy and Fast Fisher Information Matrices and Neural Tangent Kernels in PyTorch, 2021. URL <https://doi.org/10.5281/zenodo.4532597>.
- Gregory, W. G., Hogg, D. W., Blum-Smith, B., Arias, M. T., Wong, K. W. K., and Villar, S. Equivariant geometric convolutions for emulation of dynamical systems, 2024. URL <https://arxiv.org/abs/2305.12585>.
- Gruver, N., Finzi, M., Goldblum, M., and Wilson, A. G. The lie derivative for measuring learned equivariance. *arXiv:2210.02984*, 2022. URL <https://arxiv.org/abs/2210.02984>.
- Gupta, J. K. and Brandstetter, J. Towards multi-spatiotemporal-scale generalized pde modeling, 2022. URL <https://arxiv.org/abs/2209.15616>.
- He, H. and Su, W. J. The local elasticity of neural networks, 2020. URL <https://arxiv.org/abs/1910.06943>.
- Herde, M., Raonić, B., Rohner, T., Käppeli, R., Molinaro, R., de Bézenac, E., and Mishra, S. Poseidon: Efficient foundation models for pdes, 2024. URL <https://arxiv.org/abs/2405.19101>.
- Héritier, S. and Ronchetti, E. Robust bounded-influence tests in general parametric models. *Journal of the American Statistical Association*, 89(427):897–904, 1994. ISSN 0162-1459. URL <https://www.jstor.org/stable/2290914>.
- Innes, M. Don’t unroll adjoint: Differentiating ssa-form programs. *CoRR*, abs/1810.07951, 2018. URL <http://arxiv.org/abs/1810.07951>.
- Jacot, A., Gabriel, F., and Hongler, C. Neural tangent kernel: Convergence and generalization in neural networks, 2020. URL <https://arxiv.org/abs/1806.07572>.
- Kayhan, O. S. and van Gemert, J. C. On translation invariance in cnns: Convolutional layers can exploit absolute spatial location, 2020. URL <https://arxiv.org/abs/2003.07064>.
- Koh, P. W. and Liang, P. Understanding black-box predictions via influence functions, 2020. URL <https://arxiv.org/abs/1703.04730>.
- Lippe, P., Veeling, B. S., Perdikaris, P., Turner, R. E., and Brandstetter, J. Pde-refiner: Achieving accurate long rollouts with neural pde solvers, 2023. URL <https://arxiv.org/abs/2308.05732>.
- Lu, J., Ko, D., and Chang, T. The standardized influence matrix and its applications. *Journal of the American Statistical Association*, 92(440):1572–1580, 1997. ISSN 0162-1459. URL <https://www.jstor.org/stable/2965428>.
- Martens, J. New insights and perspectives on the natural gradient method. *Journal of Machine Learning Research*, 21(146):1–76, 2020. URL <http://jmlr.org/papers/v21/17-678.html>.
- Martens, J. and Grosse, R. Optimizing neural networks with kronecker-factored approximate curvature, 2020. URL <https://arxiv.org/abs/1503.05671>.
- Montoisson, A. and Orban, D. Krylov.jl: A Julia basket of hand-picked Krylov methods. *Journal of Open Source Software*, 8(89):5187, 2023. doi: 10.21105/joss.05187.
- Nguyen, T., Brandstetter, J., Kapoor, A., Gupta, J. K., and Grover, A. Climax: A foundation model for weather and climate, 2023. URL <https://arxiv.org/abs/2301.10343>.
- Ohana, R., McCabe, M., Meyer, L., Morel, R., Agocs, F. J., Beneitez, M., Berger, M., Burkhart, B., Burns, K., Dalziel, S. B., Fielding, D. B., Fortunato, D., Goldberg, J. A., Hirashima, K., Jiang, Y.-F., Kerswell, R. R., Maddu, S., Miller, J., Mukhopadhyay, P., Nixon, S. S., Shen, J., Wateaux, R., Blancard, B. R.-S., Rozet, F., Parker, L. H., Cranmer, M., and Ho, S. The well: a large-scale collection of diverse physics simulations for machine learning, 2025. URL <https://arxiv.org/abs/2412.00568>.

Pal, A. On Efficient Training & Inference of Neural Differential Equations, 2023a.

Pal, A. Lux: Explicit Parameterization of Deep Neural Networks in Julia, 2023b. URL <https://doi.org/10.5281/zenodo.7808903>.

Takamoto, M., Praditia, T., Leiteritz, R., MacKinlay, D., Alesiani, F., Pflüger, D., and Niepert, M. Pdebench: An extensive benchmark for scientific machine learning, 2024. URL <https://arxiv.org/abs/2210.07182>.

Thomas, N., Smidt, T., Kearnes, S., Yang, L., Li, L., Kohlhoff, K., and Riley, P. Tensor field networks: Rotation- and translation-equivariant neural networks for 3d point clouds. *arXiv:1802.08219*, 2018. URL <https://arxiv.org/abs/1802.08219>.

TransferLab. pyDVL, 2024. URL <https://github.com/aai-institute/pyDVL>.

Wang, R., Walters, R., and Yu, R. Approximately equivariant networks for imperfectly symmetric dynamics, 2022. URL <https://arxiv.org/abs/2201.11969>.

Wang, S., Bhartari, A. K., Li, B., and Perdikaris, P. Gradient alignment in physics-informed neural networks: A second-order optimization perspective, 2025. URL <https://arxiv.org/abs/2502.00604>.

Weiler, M., Geiger, M., Welling, M., Boomsma, W., and Cohen, T. 3d steerable CNNs: Learning rotationally equivariant features in volumetric data. *arXiv:1807.02547*, 2018. URL <https://arxiv.org/abs/1807.02547>.

Xie, Y. and Smidt, T. A tale of two symmetries: Exploring the loss landscape of equivariant models, 2025. URL <https://arxiv.org/abs/2506.02269>.

Zhang, R. Making convolutional networks shift-invariant again. In Chaudhuri, K. and Salakhutdinov, R. (eds.), *Proceedings of the 36th International Conference on Machine Learning*, volume 97 of *Proceedings of Machine Learning Research*, pp. 7324–7334. PMLR, 09–15 Jun 2019. URL <https://proceedings.mlr.press/v97/zhang19a.html>.

Zhao, B., Gower, R. M., Walters, R., and Yu, R. Improving convergence and generalization using parameter symmetries, 2024. URL <https://arxiv.org/abs/2305.13404>.

Zielinski, P., Krishnan, S., and Chatterjee, S. Weak and strong gradient directions: Explaining memorization, generalization, and hardness of examples at scale, 2020. URL <https://arxiv.org/abs/2003.07422>.

## A. Supplementary Figures

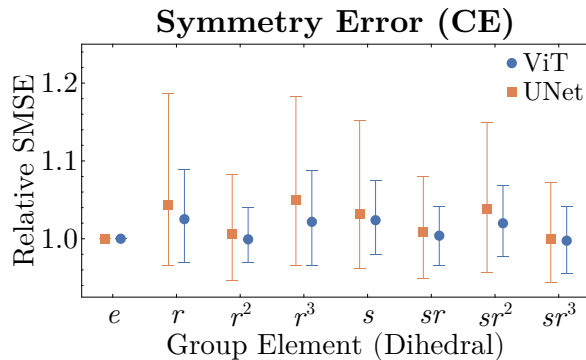


Figure 9. Dihedral (square-group  $D_4$ ) equivariance error on CE data. For each group element  $g \in D_4$  (quarter-rotations  $r$  and a reflection  $s$ ), we report the relative SMSE,  $\text{SMSE}(g \cdot x)/\text{SMSE}(x)$ , at fixed time and within class. Markers denote medians over test examples and random seeds; vertical ranges indicate inter-seed and inter-example variability. Values exceeding unity indicate symmetry breaking in the model predictions.

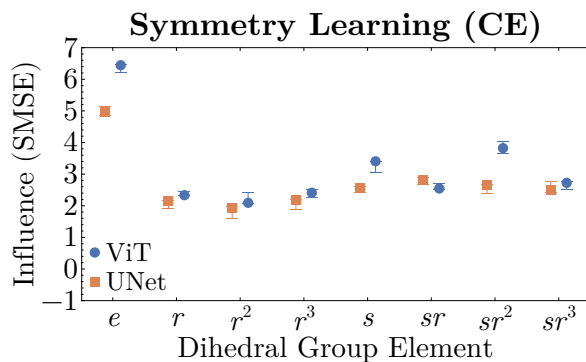


Figure 10. Dihedral group influence on CE data. Influence between an input and its square group transformed counterpart. Influence measures gradient overlap in the NTK-geometry, indicating coupling of parameter updates along the dihedral orbit. Markers denote medians; ranges indicate variability over seeds and test examples.

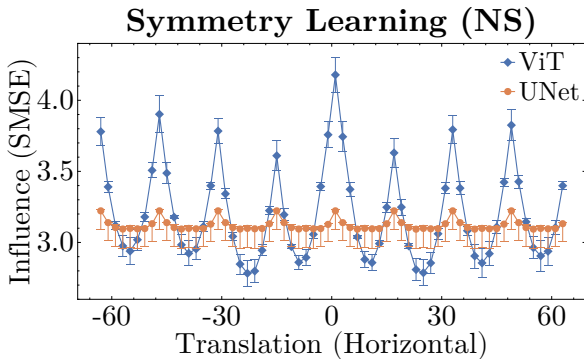


Figure 11. Horizontal-translation influence on NS data. Influence between an input and its horizontal translation. Points denote medians; ranges indicate variability over seeds and test examples.

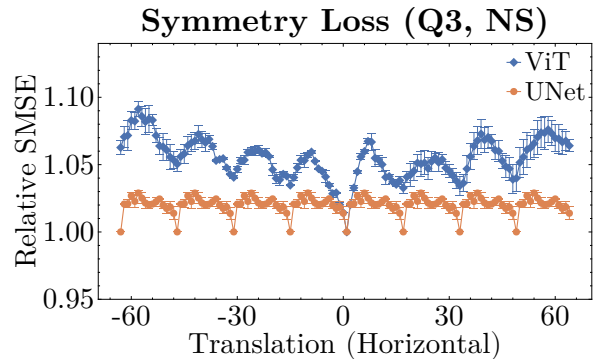


Figure 13. Horizontal-translation equivariance error on NS data (third quartile). Third-quantile relative SMSE under horizontal translations. Points denote medians across seeds; ranges emphasize upper-tail translation-induced error.

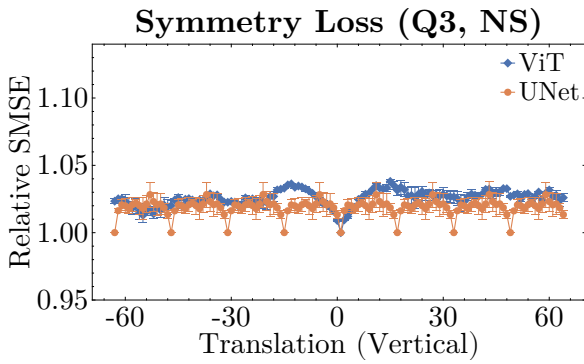


Figure 12. Vertical-translation equivariance error on NS data (third quartile). Third-quantile relative SMSE as a function of vertical translation. Points denote medians; ranges highlight upper-tail symmetry breaking.

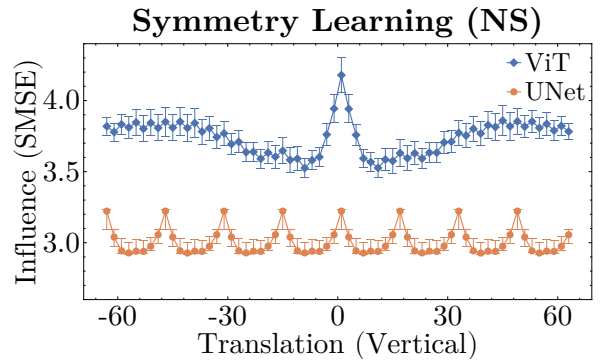


Figure 14. Vertical-translation influence on NS data. Influence between an input and its vertical translation. Points denote medians; ranges summarize variability across seeds and test examples.

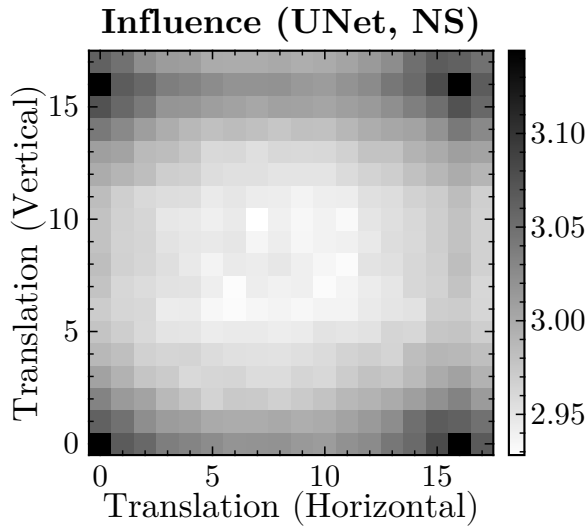


Figure 15. Translation-group influence landscape for UNet on NS data. Heatmap of Influence across joint translations quantifying how UNet parameter updates couple translated NS states.

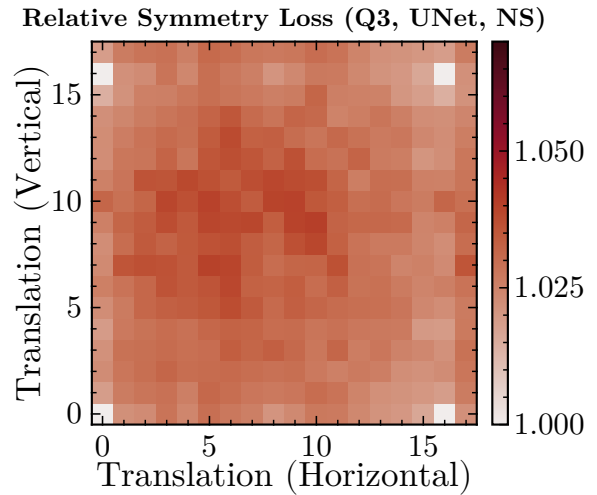


Figure 17. Translation-equivariance error landscape for UNet on NS data. Heatmap of third-quantile relative SMSE, providing a two-dimensional view of residual translation symmetry loss.

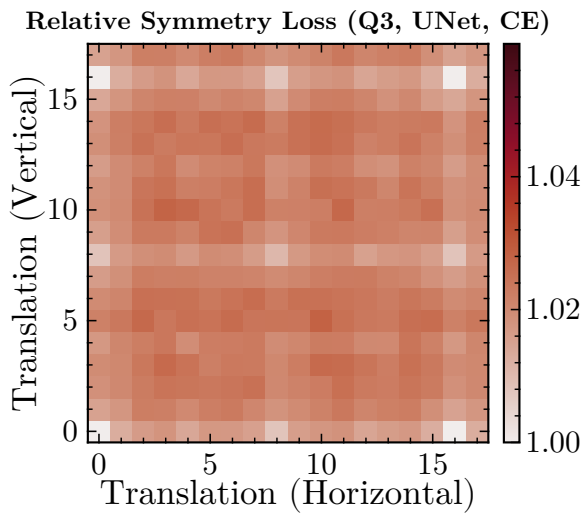


Figure 16. Translation-equivariance error landscape for UNet on CE data. Heatmap of third-quantile relative SMSE versus joint translations. Smoother structure relative to ViT reflects convolutional inductive bias modulated by multiscale pooling and upsampling. For analogous results with NS data, see Figure 17.

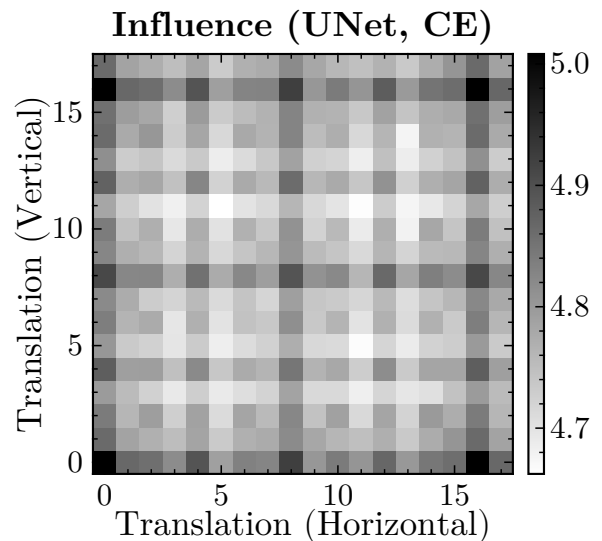


Figure 18. Translation-group influence landscape for UNet on CE data. Heatmap of influence across joint translations. Spatial structure diagnoses how UNet training updates propagate along translation orbits. For analogous results with NS data, see Figure 15.

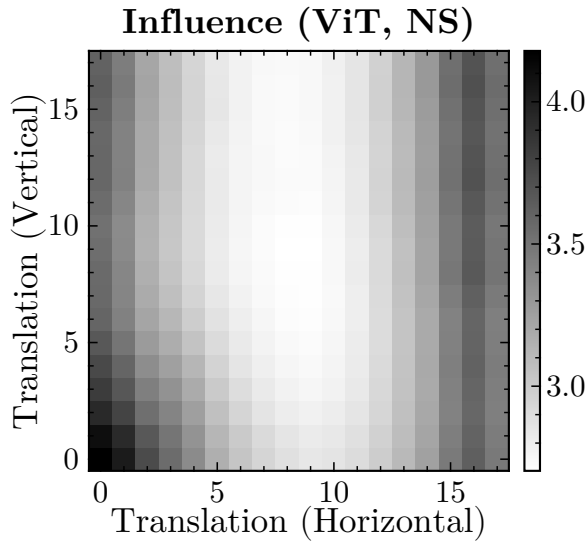


Figure 19. Translation-group influence landscape for ViT on NS data. Heatmap of Influence between an example and its translated state. Color encodes the strength of translation-orbit coupling in ViT learning dynamics.

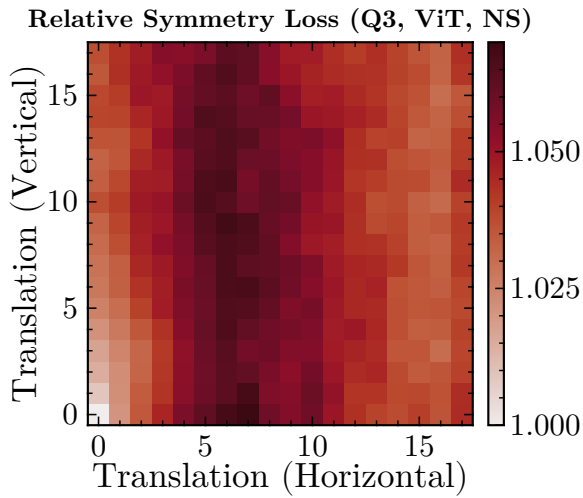


Figure 20. Translation-equivariance error landscape for ViT on NS data. Heatmap of third-quantile relative SMSE over joint translations, identifying translation pairs that induce elevated upper-tail error.